Observation of second flexural mode enhancement in graphene resonators

Observation of second flexural mode enhancement in graphene resonators

T. Chen, E. Mastropaolo, A. Bunting, R. Cheung

The enhancement of the second flexural mode in a monolayer graphene resonator by an inhomogeneous electrostatic actuation force has been observed. The devices have been fabricated by transferring the graphene onto a poly-Si/SiO_2/Si substrate whereby the poly-Si has been released to produce the graphene resonators. Enhancement of the second harmonic has been demonstrated by varying the actuation voltage, achieving amplitude enhancement up to 95% of the fundamental mode. The reported findings open new perspectives for graphene resonant sensors with enhanced sensitivity.

Introduction: Higher order resonance modes of micro and nano electromechanical resonators are of great interest because of their high sensitivity to physical quantity changes [1]. Moreover, the higher modes of resonators are crucial for the implementation of phonon lasing reminiscent of stimulated photon emission in optical lasers [2]. Resonators' harmonics can be actuated and detected using different mechanisms including piezoelectric, magnetomotive, or optical [2-4]. Odd modes (i = 1, 3, …) are activated by applying a uniform actuation force while even modes (i = 2, 4, ...) can be activated using a non-uniform force [3,4]. In nanoscale graphene resonators, higher harmonics (i > 1) have been observed only by optical actuation so far [5,6].

In this Letter, we present, for the first time, the second mode enhancement in graphene resonators by electrostatic transduction. In particular, the graphene clamped-clamped sheets have been driven into resonance by an inhomogeneous electrostatic force using frequency modulation (FM) current mixing transduction [7-9]. In this specific configuration, the amplitude of the second mode has been observed to be enhanced by up to 95% of the amplitude of the fundamental mode. The second mode enhancement observed here employing our actuation set-up holds great potential to boost the sensitivity of mass or force sensors based in graphene resonators.

Theory: The graphene resonator can be described as an Euler-Bernoulli beam with extremely small flexural stiffness, so the displacement of an infinitesimal small section of graphene can be written as [10]:

$$\sigma t_g W \frac{d^2w(x,t)}{dx^2} - \alpha \frac{dw(x,t)}{dx} = F_a(x,t) + \rho t_g W \frac{d^2w(x,t)}{dt^2} \qquad (1)$$

where α is the damping coefficient, ρ is the mass density, t_g and W are the thickness and the width of the graphene bridge, F_a is the electrostatic force, and σ is the stress in the graphene. The vertical displacement of graphene structure $w(x,t)$ can be expressed as a superposition of different mode shapes [11]:

$$w(x,t) = \sum_i \psi_i(x) y_i(t) \qquad (2)$$

where $y_i(t)$ is the time dependent periodical function associated with the amplitude of ith mode, and $\psi_i(x)$ is the spatial modal shape of the ith mode. Further, it can be shown that the magnitude of each mode depends on the term:

$$\int_0^L |F_a| \psi_i(x)\, dx \qquad (3)$$

which represents the actuation force projected onto ith mode. If the magnitude of the actuation force $|F_a|$ is uniform $|F_{a1}| = c_1$, along the resonator with length L, then

$$\int_0^L |F_{a1}| \psi_2(x)\, dx = 0 \qquad (4)$$

and therefore, the second mode will not be activated [12,13]. In the actuation set-up shown below in Fig. 1*c*, the amplitude of the FM signal drops from the drain side to the source side due to the resistance of the graphene layer. Under these conditions, the voltage difference between the graphene bridge and the substrate drops linearly from the drain end to the source end, so that the magnitude of actuation force has the form $|F_{a2}(x)| = kx + c_2$, where k and c_2 are constants. That is to say, the actuation force is inhomogeneous along the graphene resonator:

$$\int_0^L |F_{a2}| \psi_2(x)\, dx = -\frac{kL^2}{2\pi} \neq 0 \qquad (5)$$

and therefore, the second mode (i = 2) is predicted to be driven into resonance.

Fabrication and testing: The clamped-clamped resonators have been fabricated from a monolayer graphene sheet, grown by chemical vapour deposition. The quality of the graphene has been inspected by Raman spectroscopy and shows monolayer signature. The monolayer has been transferred onto a multilayer substrate consisting of poly-Si (75 nm) grown on SiO_2 (100 nm) on a Si wafer [14]. After the transfer, the graphene layer has been patterned into rectangular geometry by O_2 plasma using photoresist as etch mask. Electrical connection to the graphene layer has been formed by patterning Cr (10nm)/Au (100nm) pad electrodes at the two ends of the graphene structure using a lift-off process. Afterwards, the graphene layers have been released by removing the poly-Si sacrificial layer underneath the graphene using XeF_2 vapour. The insulating SiO_2 layer below the poly-Si layer prevents leakage from the gate to the device. Fig. 1*a* and Fig. 1*b* show a scanning electron micrograph and a schematic representation of the device, respectively. The length L, width W and thickness t_g of the device are 12 μm, 2 μm and 0.34 nm, respectively. Fig. 1*c* shows a schematic diagram of the electrostatic transduction set-up adopted to actuate the as-fabricated graphene resonators [7,13]. The amplitude of the AC voltage difference between the graphene and the substrate $V_a(x,t)$ drops from the drain end (x = 0) to the source end (x = L) due to the electrical resistance of the graphene sheet. Therefore, the electrostatic force F_a is inhomogeneous and varies along the graphene sheet as the actuation voltage V_a drops from drain to source. As a result, enhancement of the second mode of resonance is expected, (see equation 5). The sample has been tested in a vacuum chamber pumped down to 3mbar at room temperature.

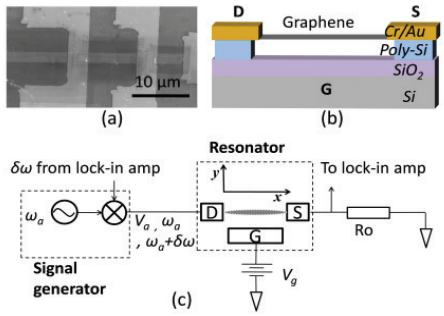

Fig. 1 *(a) Scanning electron micrograph of one of the fabricated graphene resonators. (b) Schematic diagram of the graphene resonator. The resonator is separated from the silicon substrate (back gate) by 75 nm air gap and 100 nm SiO_2. Metal electrodes contact both ends of graphene layer and serve as source and drain electrodes. (c) Circuit diagram of the frequency modulation (FM) current mixing characterisation set-up.*

Results and discussion: Fig. 2*a* shows the measured mixed current I_{mix} as a function of frequency with different actuation voltage V_a from 150 mV to 450 mV at gate voltage V_g = 0 V. Fig. 2*b* and Fig. 2*c* show the percentage peaks' amplitude change and percentage frequency shift as a function of V_a respectively.

http://dx.doi.org/10.1049/el.2015.0361
Published in: Electronics Letters
Publication date: June 2015
Publisher: the Institution of Engineering and Technology (the IET)

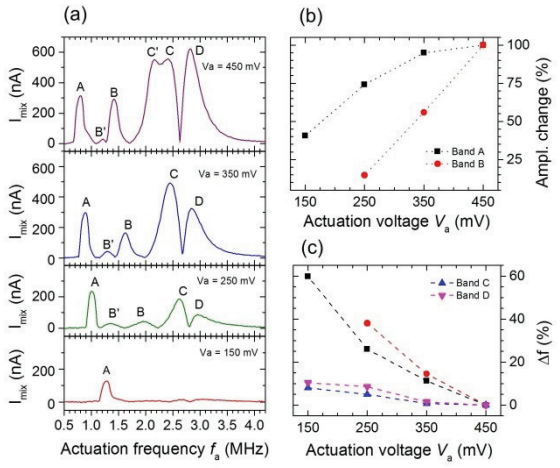

Fig. 2 *(a) Mixed current I_{mix} in the frequency range from 250 kHz to 4.5 MHz with different actuation voltages V_a (gate voltage V_g = 0 V). (b) Percentage change of peaks' amplitude and (c) percentage frequency shift Δf with respect to the frequency at V_a = 450 mV, as a function of actuation voltage V_a (gate voltage V_g = 0 V).*

Peak A at 1.01 MHz can be associated with the fundamental mode since it is activated at the lowest actuation voltage and is consistently present at higher actuation voltages. From Fig. 2*b*, the amplitude of peak A is observed to increase linearly with increasing V_a and saturates above 250 mV, probably due to nonlinear effects (see peak distortion at V_a = 350 mV and 450 mV in Fig 2*a*) [15]. Peak B appears at 1.96 MHz when V_a = 250 mV and is believed to be the second mode. It can be seen that peak B's amplitude increases linearly as V_a is increased to 450 mV, achieving an amplitude of about 95% of peak A. Under such actuation conditions, it is believed that the second mode is enhanced by the presence of the inhomogeneous actuation force F_a as a consequence of the increase of the actuation voltage V_a. As far as peaks C and D are concerned, both peaks have relatively large amplitudes that reach values greater than the amplitude of peak A for actuation voltages $V_a \geq$ 350 mV, when C' also emerges, (see Fig. 2*a*). Peaks C', C and D possibly have a spurious origin and are most likely resulting from the undercut of the device at both ends of the resonator [13]. The relatively large shift for peaks A (60%) and B (38%) to lower frequencies as V_a increases (Fig. 2*c*) can be explained by the fact that the resonant frequency ω_{ri} of a mode i is influenced by the damping coefficient n, $\omega_{ri} = \sqrt{\omega_i{}^2 - 2n^2}$, where ω_i is the undamped resonant frequency. It is most likely that the damping coefficient n increases due to nonlinear damping effects at higher resonance amplitudes as a consequence of the increase of the actuating force [8]. Under these conditions, the resonant frequency of a mode ω_{ri} shifts to lower values, which is consistent with our experimental observations.

Conclusions: Monolayer graphene resonators have been fabricated and tested. The enhancement of the second mode in the graphene electromechanical resonator by 95% of the fundamental frequency has been observed by applying an inhomogeneous electrostatic actuation force. Our report is the first demonstration of even mode activation and enhancement on nanoscale resonators using an electrostatic actuation approach. These results suggest that a significant sensitivity improvement could be possible when operating graphene resonant sensors in the second mode regime.

T. Chen, E. Mastropaolo, A. Bunting, R. Cheung *(Scottish Microelectronics Centre, The University of Edinburgh, King's Buildings, West Mains Road, EH9 3JF, Edinburgh, United Kingdom)*

Email: r.cheung@ed.ac.uk

References

1. M. K. Ghatkesar, V. Barwich, T. Braun, J.-P. Ramseyer, C. Gerber, M. Hegner, H. P. Lang, U. Drechsler, and M. Despont, 'Higher modes of vibration increase mass sensitivity in nanomechanical microcantilevers', Nanotechnology 18, 445502 (2007). doi:10.1088/0957-4484/18/44/445502
2. I. Mahboob, K. Nishiguchi, A. Fujiwara, and H. Yamaguchi, 'Phonon Lasing in an Electromechanical Resonator', Phys. Rev. Lett. 110, 127202 (2013). DOI: http://dx.doi.org/10.1103/PhysRevLett.110.127202
3. H. J. R. Westra, M. Poot, H. S. J. van der Zant, and W. J. Venstra, 'Nonlinear Modal Interactions in Clamped-Clamped Mechanical Resonators', Phys. Rev. Lett. 105, 117205 (2010). DOI: http://dx.doi.org/10.1103/PhysRevLett.105.117205
4. D. Garcia-Sanchez, A. San Paulo, M. Esplandiu, F. Perez-Murano, L. Forró, A. Aguasca, and A. Bachtold, 'Mechanical Detection of Carbon Nanotube Resonator Vibrations', Phys. Rev. Lett. 99, 085501 (2007). DOI: http://dx.doi.org/10.1103/PhysRevLett.99.085501
5. A. M. Van Der Zande, R. a Barton, J. S. Alden, C. S. Ruiz-Vargas, W. S. Whitney, P. H. Q. Pham, J. Park, J. M. Parpia, H. G. Craighead, and P. L. McEuen, 'Large-Scale Arrays of Single-Layer Graphene Resonators', Nano Lett. 10(12) , 4869 (2010). DOI: 10.1021/nl102713c
6. J. S. Bunch, A. M. van der Zande, S. S. Verbridge, I. W. Frank, D. M. Tanenbaum, J. M. Parpia, H. G. Craighead, and P. L. McEuen, 'Electromechanical Resonators from Graphene Sheets', Science 315, 490 (2007). DOI: 10.1126/science.1136836
7. V. Gouttenoire, T. Barois, S. Perisanu, J.-L. Leclercq, S. T. Purcell, P. Vincent, and A. Ayari, 'Digital and FM Demodulation of a Doubly Clamped Single-Walled Carbon-Nanotube Oscillator: Towards a Nanotube Cell Phone', Small 6, 1060 (2010). DOI: 10.1002/smll.200901984
8. A. Eichler, J. Moser, J. Chaste, M. Zdrojek, I. Wilson-Rae, and A. Bachtold, 'Nonlinear damping in mechanical resonators made from carbon nanotubes and graphene', Nat. Nanotechnol. 6, 339 (2011). doi:10.1038/nnano.2011.71
9. J. Chaste, A. Eichler, J. Moser, G. Ceballos, R. Rurali, and A. Bachtold, 'A nanomechanical mass sensor with yoctogram resolution', Nat. Nanotechnol. 7, 301 (2012). doi:10.1038/nnano.2012.42
10. P. Hagedorn and A. DasGupta, Vibrations and Waves in Continuous Mechanical Systems (John Wiley & Sons, 2007), pp. 116–120.
11. E. Blokhina, J. Pons, J. Ricart, O. Feely, and M. D. Pumar, 'Control of MEMS vibration modes with pulsed digital Oscillators, part I Theory', IEEE Trans. Circuits Syst. I. 57, 1865 (2010). DOI: 10.1109/TCSI.2009.2038541
12. H. Peng, C. Chang, S. Aloni, T. Yuzvinsky, and A. Zettl, 'Ultrahigh Frequency Nanotube Resonators', Phys. Rev. Lett. 97, 087203 (2006). DOI: http://dx.doi.org/10.1103/PhysRevLett.97.087203
13. C. Chen, S. Rosenblatt, K. I. Bolotin, W. Kalb, P. Kim, I. Kymissis, H. L. Stormer, T. F. Heinz, and J. Hone, 'Performance of monolayer graphene nanomechanical resonators with electrical readout', Nat. Nanotechnol. 4, 861 (2009). doi:10.1038/nnano.2009.267
14. T. Chen, E. Mastropaolo, A. Bunting, T. Stevenson, and R. Cheung, 'Optimization of the visibility of graphene on poly-Si film by thin-film optics engineering', J. Vac. Sci. Technol. B 30, 06FJ01 (2012). DOI: 10.1116/1.4758760
15. K. L. Ekinci and M. L. Roukes, 'Nanoelectromechanical systems', Rev. Sci. Instrum. 76, 061101 (2005). DOI: 10.1063/1.1927327

http://dx.doi.org/10.1049/el.2015.0361

Published in: Electronics Letters
Publication date: June 2015
Publisher: the Institution of Engineering and Technology (the IET)